Giant field enhancement in photonic resonant lattices

V. Mocella and S. Romano
CNR-IMM-Unità di Napoli, Via P. Castellino 111, 80131 Napoli, Italy
(Received 28 April 2015; revised manuscript received 15 September 2015; published 12 October 2015)

A giant field enhancement factor, defined as the ratio between the intensity of the resonant and the incident fields, is achievable in a photonic crystal (PhC) slab realized in a low contrast dielectric medium. The key point is the careful control of some parameters, first among all the slab thicknesses, which allows for stabilizing the coupling resonant mechanism. These modes are closely correlated with symmetry-protected bound states in continuum. Our study proves, in frequency as in time domain, that such modes can be excited with a normal incident beam and that the giant resonant enhanced field starts to grow and is established after more than 10^5-cycle time. Up to six orders of magnitude of field enhancement distributed along all the slab is achievable, making it easier to use in many applications than localized enhancement.

DOI: 10.1103/PhysRevB.92.155117 PACS number(s): 42.70.Qs, 78.20.Bh, 78.20.Ci

Local enhancement of the electric field in photonic structures can be very efficient to manipulate light and boost nonlinear phenomena and is extremely appealing for a wide range of applications, such as optical detection [1,2], single-molecule sensing [3,4], and energy conversion [5]. Generally, high-field enhancement factors can be generated in metallic nanoentities, such as metallic nanostructures [6], nanoparticles [3] or nanoantennas [7], by exploiting *surface-plasmon polaritons* (SPPs), which propagate along a metal/dielectric plane interface and *localized surface-plasmon polaritons* (LSPPs), which involve other geometries, such as metallic particles. In particular, the electric field of a bound (nonradiative) SPP has a peak at the interface and decays exponentially in both media. Devices based on SPPs have been developed for label-free chemical and biological sensing [6,8–13], allowing the study of the interactions between a biomolecule and its specific target with very high sensitivity and low detection limits. Another useful application of plasmon resonances in optical biosensing is represented by surface-enhanced Raman spectroscopy [14,15] where local plasmon states are excited by the incident light near metallic nanoparticles, allowing the enhancement of the Raman signal coming from investigated analytes [15]. The field enhancement factor is about 10^4–10^6, and in metallic nanoparticles the degree of confinement is strongly dependent on particles' size, shape, composition, and relative arrangement.

Alternatively a large electromagnetic field can be produced and confined in the gap region of metallic nanoantennas where two metallic structures are separated by a short distance. In this case the enhancement factor depends on the structures shape and on their interdistances and can reach the value of 10^6 in a gap of 1 nm [16,17].

Nevertheless, the strong electromagnetic-field enhancement and the sensitivity upon changes in the refractive index at metal/dielectric interfaces are penalized by the presence of the metallic structures. In fact the large absorption at optical frequencies in metals, the local heating, and the heat dissipation result in a broadening of the surface-plasmon resonance profile and in probable biological material damage. Therefore, the possibility of managing surface electromagnetic states, mimicking surface-plasmon resonances in terms of spatial localization, high-field intensity, and dispersion characteristics while avoiding the metallic losses [18] would be of great interest.

Plasmonic metallic materials are not the only way to achieve optical-field enhancement and, in the past years, the field enhancement in a structured dielectric surface has gained increasing attention [19–23]. In particular an electromagnetic wave of a specific frequency can be localized and trapped by structures, such as photonic [24–26] and plasmonic [27] nanocavities, in which outgoing waves are completely forbidden. Very recently [28,29] it has been demonstrated that perfect light confinement can be achieved in PhC slabs because of a particular type of localized state: a *bound state in the continuum* (BIC) [30–32]. Historically, BICs first appeared in quantum systems thanks to von Neumann and Wigner [33] who interpreted the phenomenon as the interference of resonances in direct and via the continuum channels. Hereafter it was demonstrated that this effect affects not only the quantum systems, but also many areas of physics, including photonics [34–37] and acoustic waves [38].

In the following we show that a lattice in a thin low contrast dielectric layer can exhibit an extremely large field enhancement up to six orders of magnitude larger than the intensity of the incident beam. Specifically, the finite dimension of a PhC slab introduces new characteristics compared to an ideal two-dimensional (2D) photonic crystal composed by infinitely long dielectric cylinders or holes. In general over the light line the band structure is complex because modes are leaky. However, in correspondence of some crucial symmetric points, symmetries associated with complex band structures can correspond to true infinite lifetime modes, above the light line [39]. These modes represent a special case for the PhC slab where bound states exist above the light line [40]. Since nonlinear effects are a function of the intensity and in some cases are proportional to the field intensity (as for the Raman effect), the enhancement discussed in the following can really be defined as giant and has no equivalence in other resonant dielectric structures. Moreover, the bound-state stabilization occurs when the thickness parameter is such to guarantee the matching between the PhC resonance frequency and the standing wave frequency in the structure. This can be considered the equivalent of the stabilization obtained by optimizing the distance of coupled grating in Ref. [35].

Lattice resonances are an inherent property of the periodic structure and are independent of the external excitation. In particular, some modes with infinite lifetimes can exist at

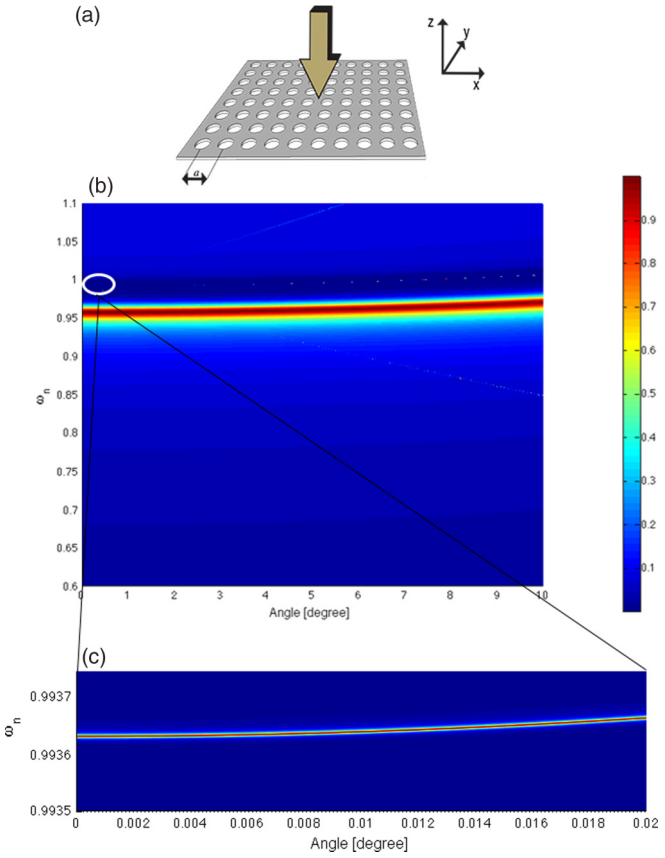

FIG. 1. (Color online) (a) Sketch of the photonic crystal consisting of a square lattice of holes in a material with a refractive index equal to 2. The sample is designed in order to have resonance modes at normal incident directions. (b) Calculated reflectivity by means of RCWA: In addition to the principal modes, a band with a very sharp profile appears close to normal incidence (see the zoom). $\omega_n = a/\lambda$ is the normalized frequency.

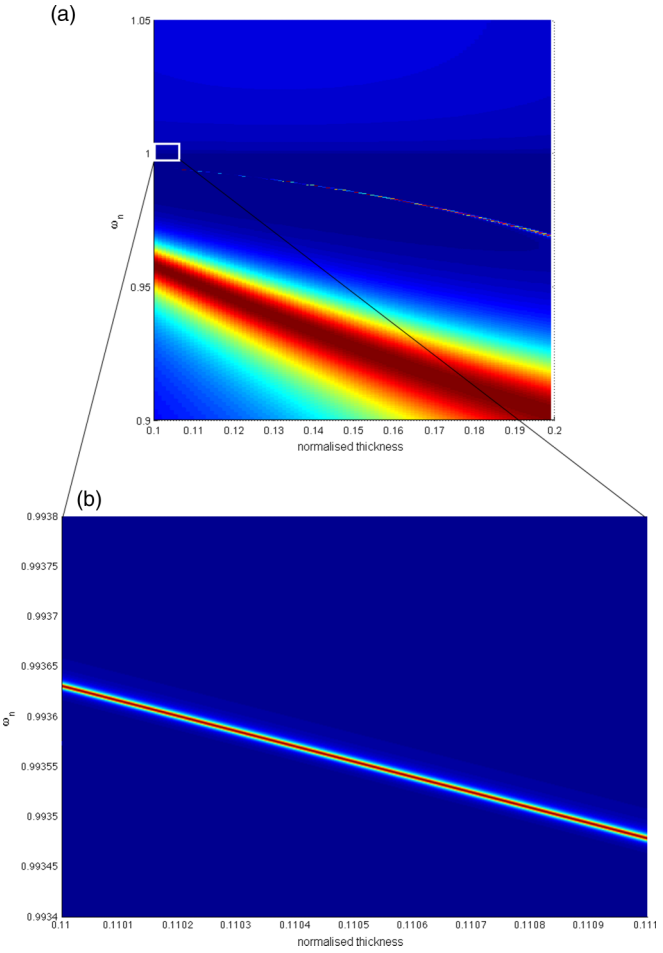

FIG. 2. (Color online) (a) Calculated reflectivity as a function of normalized photonic crystal thickness and (b) a zoom of the bound-state modes region.

normal incidence, i.e., in the Γ point of the Brillouin zone where symmetry protects such modes preventing the radiation coupling outside the photonic crystal [39,41]. Some symmetry consideration can help in the modes' analysis. In particular, let us now be reminded that in the Γ point of the Brillouin zone a square lattice photonic crystal slab as in Fig. 1(a) has a C_{4v} point-group symmetry inside the lattice plane and a C_{1h} symmetry in the direction normal to the lattice plane, corresponding to even/odd symmetry with respect to such a mirror plane. The symmetry condition matching allows only doubly degenerate modes to couple with a normal incident wave, and for such a reason the guided mode resonances are always doubly degenerate [42].

The numerical study of the excited modes in the structure had been performed by using a full tridimensional rigorous coupled wave approach (RCWA) based on a Fourier modal expansion [43]. The designed structure consists of a square lattice of holes with a radius of $r/a = 0.25$ in a material with a refractive index equal to 2. Figure 1(b) shows the calculated band. At first analysis, the principal band around the normalized frequency 0.96 is identified ($\omega_n = a/\lambda$, normalized frequency). However, by zooming the region around the incident angle $\theta = 0^\circ$ [see Fig. 1(c)] extremely narrow bands appear around the frequency 0.995. In order to highlight them a high-resolution numerical calculation of around 10^{-5} in terms of normalized frequency is required.

Moreover, the reflectivity as a function of the normalized slab thickness for the normal incident beam, i.e., directed along the z axis, is analyzed by considering the incident electric field as directed along the x axis (see Fig. 2). Also in this case different bands are visible, the modes clearly identified around $\omega_n = 0.96$, and the modes around $\omega_n = 0.995$ with an extremely narrow profile as a function of the thickness [Fig. 2(b)]. The first mode band clearly identifies guided mode resonances, i.e., resonances due to the coupling between the external radiation and the long-living radiative states localized within a PhC. In particular, around the Γ point and close to the first Bragg condition, agreeing with previously highlighted symmetries, a 2D square lattice has four dominant guided modes for each polarization associated with the $(\pm 1,0)$ and $(0,\pm 1)$ lattice points. Close to the normalized frequencies 1 (i.e., $a \sim \lambda$) a very high quality resonance band can be identified [see Fig. 2(b)]. In particular, the reflectivity evaluated at normal incidence for a normalized thickness of $0.12a$ has a very narrow peak with a quality factor as high as $Q = 2 \times 10^5$.

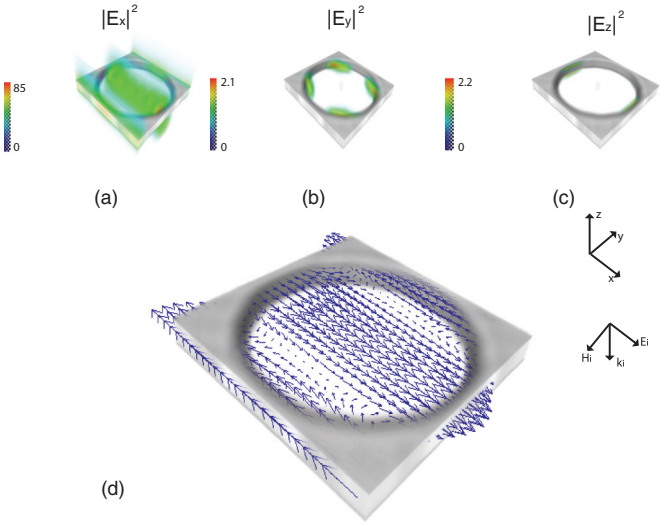

FIG. 3. (Color online) The electric field for a normal incident beam in correspondence of $\omega_n = 0.96$ calculated by using the RCWA. The electric-field intensity along the x, y, and z directions (a)–(c). The electric-field vector in the slab median plane (d).

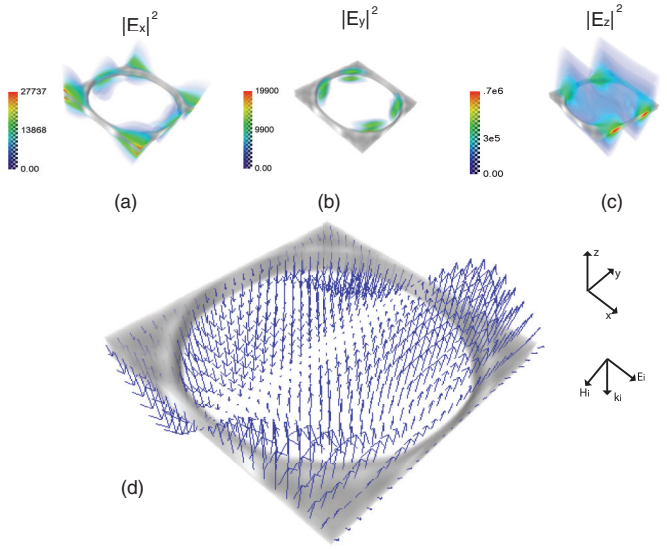

FIG. 4. (Color online) The electric field for a normal incident beam in correspondence of $\omega_n = 0.995$ calculated by using the RCWA. The electric-field intensity along the x, y, and z directions (a)–(c). The electric-field vector in the slab median plane (d).

Let us now analyze the electric-field distribution within the PhC slab in correspondence of the two bands of Fig. 2(a). In general, all eigenstates in a slab contain a mixture between transverse magnetic [(TM), the magnetic field is confined to the xy plane, see Fig. 1(a)] and transverse electric [(TE), the electric field is confined to the xy plane] modes so that it is not possible to rigorously define a TE or a TM polarization. However, it is still possible to distinguish between TM-like or TE-like in modes according to the dominant component of the excited electric fields (see Ref. [44]). Although at normal incidence purely 2D TE and TM modes are degenerate, in a 2D slab modes split because of the different effective indices of the slab for the two polarizations, in agreement with the previous analysis [39].

In correspondence of $\omega_n = 0.96$ in the middle of the larger band in Fig. 2, the electric field is almost completely directed along the x direction, i.e., parallel to the incident beam. This is illustrated in Figs. 3(a)–3(c) where the intensity of the electric field along the different directions is shown. The maximum field intensity in the x direction is about 85 times the intensity of the incident beam, which can be useful for some applications, but it is not enough to enhance weak effects, such as the Raman signal emission. Figure 3(d) shows the three-dimensional picture of the electric-field vector on the median plane of the slab. The electric field is directed along the x direction, and, residing on the (x,y) plane of the lattice, this resonance can be classified as TE-like.

In Fig. 4 the electric field of the very narrow resonance in correspondence of $\omega_n = 0.995$ is shown. As illustrated in Figs. 4(a)–4(c), the field is strongly enhanced not only on the (x,y) plane where the incident field lies, but also along the z direction, i.e., longitudinal to the incident beam direction. In particular, along the z direction the field intensity is about two orders of magnitude higher than the intensity along the x direction and is six orders of magnitude larger than the incident beam, which is therefore particularly appealing for amplifying most of the nonlinear phenomena. In this case, the electric field is essentially directed along the z direction as shown in Fig. 4(d), and the modes corresponding to the narrow bands of Figs. 1 and 2 are then TM-like modes. These results can find interesting applications in the control of the radiation field in absorption-free media, avoiding the typical limitation of the metallic plasmonic structure. In addition, in this case the field enhancement is distributed in a large area despite what happens in other nanostructures with high-field enhancement, such as nanoantennas or nanocavities [45]. We underline that in the case of normal incidence the resonant electric field is parallel to the incident wave vector. The resonant frequency is just under the excitation of high order in the lattice which corresponds to $\omega_n = 1$ for a normal incidence in a square lattice. Due to the conservation of the tangential component of the wave vector and the electric field, zero in both cases, the mode cannot couple with radiative modes outside of the PhC slab where longitudinal modes are not permitted. It is therefore a real bound state within the continuum of radiation [35,46].

To understand the temporal evolution of these bound resonances a further study is carried out using a time-domain simulation with a finite difference time-domain (FDTD) algorithm. Figure 5 shows the electric field as a function of the time in three points of the elementary cell. In an arbitrary point out of any symmetry of lattice A, the modulus of the field amplitude along the z axis evolves very slowly to stabilize its steady-state value after about 2×10^4 periods. In two symmetric points B and C, the field has a rather typical evolution of resonances. After 2×10^5 periods, the field begins to grow steadily in order to evolve to the steady-state regime. The FDTD analysis confirms in the time domain the results obtained in the frequency domain with the RCWA approach, clarifying that the resonant z component grows very slowly in the elementary cell and is negligible for 1000 periods.

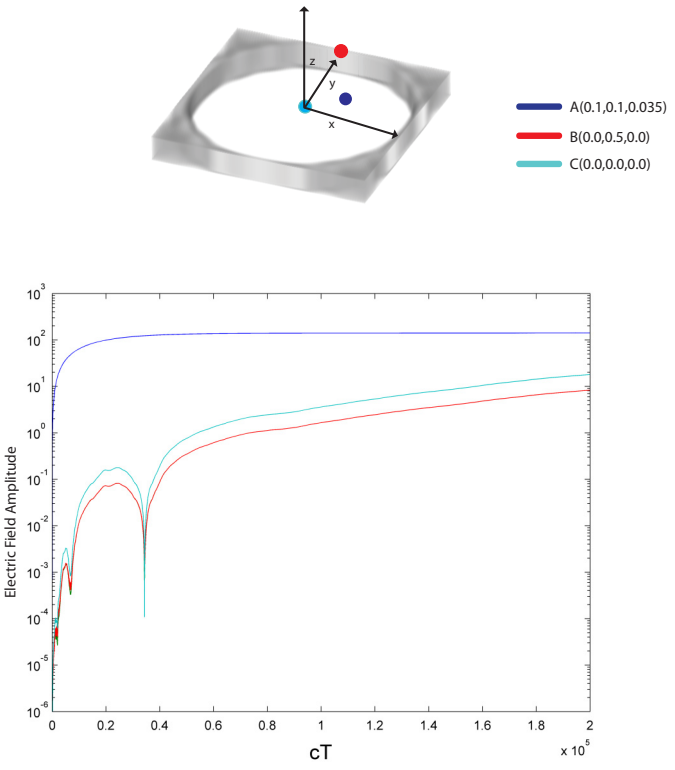

FIG. 5. (Color online) The modulus of the amplitude of the electric field along the z direction on the logarithmic scale. The incident beam is in a normal direction and is calculated in correspondence of $\omega_n = 0.995$ calculated with a FDTD algorithm in three different points A, B, C as a function of the normalized simulation time cT, where c is the speed of light in vacuum and T is the time during simulation.

This is not surprising because the E_z component is parallel to the incident beam that is along the z direction. This field component is excited in correspondence of the $(\pm 1, 0)$ and $(0, \pm 1)$ orders of the square lattice where the wave vectors are directed along the x and y directions, respectively. As we underlined before, such orders are evanescent in the air because the frequency is slightly under the coupling with the first diffraction orders in vacuum. The conservation of the tangential component of the electric field, which is incident along the x direction, makes possible the electric-field excitation inside the slab initially directed along the x direction. It is necessary for a very long time in order to establish the electric field along the z direction, corresponding to the resonant components of the Ewald-Bloch expansion of the wave field inside the PhC.

We presented a full description of the wave-field components of the resonant electric field in a photonic crystal slab in correspondence of bound modes embedded in continuum of the radiation in vacuum. These resonances have a predicted an infinite lifetime connected with a huge field enhancement and are protected by the lattice symmetry so they exist in the slab and cannot couple with external radiation. However, the numerical simulation approximations and fabrication imperfections partially break this symmetry allowing the coupling of the external incoming beam. A comprehensive numerical analysis, both in time and in frequency domain, shows that such modes can be excited by a normal incident beam and can reach a giant field enhancement of about 10^6 distributed over all the structure. These remarkable results set the foundation for immediate applications in several fields, such as high sensitivity refractive-index sensing and surface enhanced Raman spectroscopy, and can play a key role in some optical phenomena, such as nonlinear effects and fluorescence emission enhancement.

[1] A. D. McFarland and R. P. Van Duyne, Single silver nanoparticles as real-time optical sensors with zeptomole sensitivity, Nano Lett. **3**, 1057 (2003).

[2] P. K. Jain, K. S. Lee, I. H. El-Sayed, and M. A. El-Sayed, Calculated absorption and scattering properties of gold nanoparticles of different size, shape, and composition: Applications in biological imaging and biomedicine, J. Phys. Chem. B **110**, 7238 (2006).

[3] J. Beermann, S. M. Novikov, K. Leosson, and S. I. Bozhevolnyi, Surface enhanced Raman imaging: Periodic arrays and individual metal nanoparticles, Opt. Express **17**, 12698 (2009).

[4] C. E. Talley, J. B. Jackson, C. Oubre, N. K. Grady, C. W. Hollars, S. M. Lane, T. R. Huser, P. Nordlander, and N. J. Halas, Surface-enhanced Raman scattering from individual Au nanoparticles and nanoparticle dimer substrates, Nano Lett. **5**, 1569 (2005).

[5] Z. Wang, P. Tao, Y. Liu, H. Xu, Q. Ye, H. Hu, C. Song, Z. Chen, W. Shang, and T. Deng, Rapid charging of thermal energy storage materials through plasmonic heating, Sci. Rep. **4**, 6246 (2014).

[6] E. M. Larsson, J. Alegret, M. Käll, and D. S. Sutherland, Sensing characteristics of NIR localized surface plasmon resonances in gold nanorings for application as ultrasensitive biosensors, Nano Lett. **7**, 1256 (2007).

[7] A. E. Krasnok, I. S. Maksymov, A. I. Denisyuk, P. A. Belov, A. E. Miroshnichenko, C. R. Simovski, and Y. S. Kivshar, Optical nanoantennas, Phys.-Usp. **56**, 539 (2013).

[8] X. Guo, Surface plasmon resonance based biosensor technique: A review, J. Biophoton. **5**, 483 (2012).

[9] P.-Y. Chung, T.-H. Lin, G. Schultz, C. Batich, and P. Jiang, Nanopyramid surface plasmon resonance sensors, Appl. Phys. Lett. **96**, 261108 (2010).

[10] T.-Y. Liu, K.-T. Tsai, H.-H. Wang, Y. Chen, Y.-H. Chen, Y.-C. Chao, H.-H. Chang, C.-H. Lin, J.-K. Wang, and Y.-L. Wang, Functionalized arrays of Raman-enhancing nanoparticles for capture and culture-free analysis of bacteria in human blood, Nat. Commun. **2**, 538 (2011).

[11] X. Yin and L. Hesselink, Goos-Hanchen shift surface plasmon resonance sensor, Appl. Phys. Lett. **89**, 261108 (2006).

[12] R. Slavík and J. Homola, Ultrahigh resolution long range surface plasmon-based sensor, Sens. Actuators, B **123**, 10 (2007).

[13] M. Nirschl, F. Reuter, and J. Vörös, Review of transducer principles for label-free biomolecular interaction analysis, Biosensors **1**, 70 (2011).

[14] J. Kneipp, H. Kneipp, and K. Kneipp, SERS–a single-molecule and nanoscale tool for bioanalytics, Chem. Soc. Rev. **37**, 1052 (2008).

[15] J. Kneipp, H. Kneipp, M. McLaughlin, D. Brown, and K. Kneipp, In vivo molecular probing of cellular compartments with gold nanoparticles and nanoaggregates, Nano Lett. **6**, 2225 (2006).

[16] L. Zhou, Q. Gan, F. J. Bartoli, and V. Dierolf, Direct near-field optical imaging of UV bowtie nanoantennas, Opt. Express **17**, 20301 (2009).

[17] M. D. Wissert, C. Moosmann, K. S. Ilin, M. Siegel, U. Lemmer, and H.-J. Eisler, Gold nanoantenna resonance diagnostics via transversal particle plasmon luminescence, Opt. Express **19**, 3686 (2011).

[18] D. Lepage, A. Jiménez, J. Beauvais, and J. J. Dubowski, Conic hyperspectral dispersion mapping applied to semiconductor plasmonics, Light: Sci. Appl. **1**, e28 (2012).

[19] L. K. Ausman and G. C. Schatz, Whispering-gallery mode resonators: Surface enhanced Raman scattering without plasmons, J. Chem. Phys. **129**, 054704 (2008).

[20] C.-L. Zou, J.-M. Cui, F.-W. Sun, X. Xiong, X.-B. Zou, Z.-F. Han, and G.-C. Guo, Photonic bound state in the continuum for strong light-matter interaction, arXiv:1305.5297.

[21] S. Romano, S. Cabrini, I. Rendina, and V. Mocella, Guided resonance in negative index photonic crystals: A new approach, Light: Sci. Appl. **3**, e120 (2014).

[22] G. N. Malheiros-Silveira, G. S. Wiederhecker, and H. E. Hernández-Figueroa, Dielectric resonator antenna for applications in nanophotonics, Opt. Express **21**, 1234 (2013).

[23] G. D'Aguanno, N. Mattiucci, M. J. Bloemer, R. Trimm, N. Aközbek, and A. Alù, Frozen light in a near-zero index metasurface, Phys. Rev. B **90**, 054202 (2014).

[24] S. Noda, A. Chutinan, and M. Imada, Trapping and emission of photons by a single defect in a photonic bandgap structure, Nature (London) **407**, 608 (2000).

[25] Y. Akahane, T. Asano, B.-S. Song, and S. Noda, High-Q photonic nanocavity in a two-dimensional photonic crystal, Nature (London) **425**, 944 (2003).

[26] K. Hirose, Y. Liang, Y. Kurosaka, A. Watanabe, T. Sugiyama, and S. Noda, Watt-class high-power, high-beam-quality photonic-crystal lasers, Nat. Photonics **8**, 406 (2014).

[27] B. Min, E. Ostby, V. Sorger, E. Ulin-Avila, L. Yang, X. Zhang, and K. Vahala, High-Q surface-plasmon-polariton whispering-gallery microcavity, Nature (London) **457**, 455 (2009).

[28] J. Lee, B. Zhen, S.-L. Chua, W. Qiu, J. Joannopoulos, M. Soljačić, and O. Shapira, Observation and Differentiation of Unique High-Q Optical Resonances Near Zero Wave Vector in Macroscopic Photonic Crystal Slabs, Phys. Rev. Lett. **109**, 067401 (2012).

[29] Y. Yang, C. Peng, Y. Liang, Z. Li, and S. Noda, Analytical Perspective for Bound States in the Continuum in Photonic Crystal Slabs, Phys. Rev. Lett. **113**, 037401 (2014).

[30] B. Zhen, C. W. Hsu, L. Lu, A. D. Stone, and M. Soljačić, Topological Nature of Optical Bound States in the Continuum, Phys. Rev. Lett. **113**, 257401 (2014).

[31] M. Zhang and X. Zhang, Ultrasensitive optical absorption in graphene based on bound states in the continuum, Sci. Rep. **5**, 8266 (2015).

[32] C. W. Hsu, B. Zhen, S.-L. Chua, S. G. Johnson, J. D. Joannopoulos, and M. Soljačić, Bloch surface eigenstates within the radiation continuum, Light: Sci. Appl. **2**, e84 (2013).

[33] J. von Neumann and E. P. Wigner, Über merkwürdige diskrete Eigenwerte, Phys. Z. **30**, 465 (1929).

[34] Y. Plotnik, O. Peleg, F. Dreisow, M. Heinrich, S. Nolte, A. Szameit, and M. Segev, Experimental Observation of Optical Bound States in the Continuum, Phys. Rev. Lett. **107**, 183901 (2011).

[35] D. C. Marinica, A. G. Borisov, and S. V. Shabanov, Bound States in the Continuum in Photonics, Phys. Rev. Lett. **100**, 183902 (2008).

[36] M. I. Molina, A. E. Miroshnichenko, and Y. S. Kivshar, Surface Bound States in the Continuum, Phys. Rev. Lett. **108**, 070401 (2012).

[37] E. N. Bulgakov and A. F. Sadreev, Bound states in the continuum in photonic waveguides inspired by defects, Phys. Rev. B **78**, 075105 (2008).

[38] R. Porter and D. V. Evans, Embedded Rayleigh-Bloch surface waves along periodic rectangular arrays, Wave Motion **43**, 29 (2005).

[39] P. Paddon and J. Young, Two-dimensional vector-coupled-mode theory for textured planar waveguides, Phys. Rev. B **61**, 2090 (2000).

[40] C. W. Hsu, B. Zhen, J. Lee, S.-L. Chua, S. G Johnson, J. D. Joannopoulos, and M. Soljačić, Observation of trapped light within the radiation continuum, Nature (London) **499**, 188 (2013).

[41] T. Ochiai and K. Sakoda, Dispersion relation and optical transmittance of a hexagonal photonic crystal slab, Phys. Rev. B **63**, 125107 (2001).

[42] K. Sakoda, *Optical Properties of Photonic Crystals*, Springer Series in Optical Sciences (Springer, Berlin, 2005).

[43] N. Chateau and J.-P. Hugonin, Algorithm for the rigorous coupled-wave analysis of grating diffraction, J. Opt. Soc. Am. A **11**, 1321 (1994).

[44] J. D. Joannopoulos, S. G. Johnson, J. N. Winn, and R. D. Meade, *Photonic Crystals: Molding the Flow of Light*, 2nd ed. (Princeton University Press, Princeton, 2007).

[45] S. A. Maier, Plasmonic field enhancement and SERS in the effective mode volume picture, Opt. Express **14**, 1957 (2006).

[46] J. M. Foley, S. M. Young, and J. D. Phillips, Symmetry-protected mode coupling near normal incidence for narrow-band transmission filtering in a dielectric grating, Phys. Rev. B **89**, 165111 (2014).